Medical Research Archives

European Society of Medicine

OPEN ACCESS

Published: August 31, 2023

Citation: Poiate, I.A.V.P., et al., 2023. Abfraction lesion in central incisor tooth: displacement and stress evaluation by laser speckle and finite element analysis, Medical Research Archives, [online] 11(8). https://doi.org/10.18103/mra.v11i8.4220

DOI: https://doi.org/10.18103/mra.v11i8.4220

ISSN: 2375-1924

RESEARCH ARTICLE

Abfraction lesion in central incisor tooth: displacement and stress evaluation by laser speckle and finite element analysis

Isis Andrea Venturini Pola Poiate[1*], Mikiya Muramatsu[2], Matsuyoshi Mori[2], Tomie Toyota de Campos[2], Kiyofumi Matsuda[3], Marcio André Prieto Aparicio Lopez[4], Edgard Poiate Junior[5]

[1]Fluminense Federal University, Nova Friburgo/RJ, Brazil.
[2]University of São Paulo, São Paulo/SP, Brazil.
[3]National Institute of Advanced Industrial Science and Technology, Chiyoda-ku/Tokyo, Japan.
[4]Nuclear and Energy Research Institute, São Paulo/SP, Brazil.
[5]Rio de Janeiro State University, Nova Friburgo/RJ, Brazil.

*poiate@yahoo.com

ABSTRACT

The aim of this study was to evaluate the displacement and stress distribution in the cervical region of a mandibular central incisor tooth (MCIT) within wedge-shaped lesion simulating abfraction lesion by means of Laser Speckle (LS) and 3D Finite Element Analysis (FEA) and then compared. One experimental setup was assembled with a MCIT attached in resin and submitted to the LS. An increasing static load from 12.1 to 42.1N was applied in incisal buccal slope at 15° in relation to the tooth's long axis. A 3D numerical model with linear tetrahedral elements and homogeneous, linear and isotropic behavior was built with the same boundary conditions of the experimental setup. The LS present higher displacement in the wedge-shaped lesion than the FEA, but both had an excellent agreement in the displacement direction. The LS show a nonlinear behavior from 32.1N. The FEA has presented higher tensile stresses at the root dentin. In the FEA cementoenamel junction area, tensile stress isn't exceeding the enamel's tensile strength, under simulated conditions. It was concluded that LS is a faster tool and acceptable when studying the quantitative displacement of the biomechanical behavior in MCIT, and FEA is appropriate for the quantitative stress analysis, and both bring important results of the stress and displacement that are fundamental in planning preventive and restorative approach in non-carious cervical lesions.

Keywords: speckle, displacement, finite elements, stress, abfraction, tooth.

1. Introduction:

A Non-carious cervical lesions (NCCL) is broadly defined as the loss of tooth substance that occurs in the absence of carious mechanisms at the cementoenamel junction (CEJ) of a tooth[1] Among them, attrition is defined as the loss of enamel, dentin, or restoration by tooth-to-tooth contact. Erosion is the loss of dental hard tissues by chemical action, not involving bacteria, and are classified according to the source of the acid, as either intrinsic (acids originate in the stomach and are associated with eating disorders) or extrinsic (acids contained in dietary components). Abrasion is the loss of tooth substance from factors other than tooth contact[2] Abfraction lesions present primarily at the cervical region of the dentition and are typically wedge-shaped, with sharp internal and external line angles.

A number of theories have arisen to explain the etiology of abfraction; yet, the real causes remain obscure, as is reflected by the contradictory terminology used in literature[3] Acidic and abrasive processes have been documented as etiological factors[4], but the role of mechanical tension from occlusal loads is the most accepted theory[5-9], explaining abfraction as a consequence of tooth deflection caused by excessive occlusal forces. During tooth deflection, tensile and compression forces are generated in the cervical region of the tooth, causing rupture of the union between hydroxyapatite crystals, leading to the formation of a crack and eventually to enamel loss[4-10] The cyclic tensile/compression stress may reach a strength limits and lead a hydroxyapatite crystal disrupts at the cervical area, rendering it were susceptible to mechanical and chemical degradation[11.]

Studies have been attributing the failure of cervical restorations in the abfraction[12,13], because those lesions frequently present margins located in enamel and dentine, and associated to the occlusal eccentric forces represent a challenge for restoring procedures[14,15] The accumulated stresses in that area have been told as responsible by the adhesion failure, allowing the appearance of rifts and penetration of fluids and bacteria, that characterize the microinfiltration[16,17], taking to the retention loss[8,13,14,18,19] and to displacement[8,13]. The decision in restoring the cervical defects has the objective of strengthening the tooth, to reduce the stress concentration and the flexing, to reduce the progression of the lesion and the inherent problems[20] As the cervical restorations are subject not only to the masticatory forces, but also to small occlusal maladjustments or interferences[21], the understanding of the biomechanics of the forces about the restorations would facilitate the selection of materials and it would improve this prognostic[6] Therefore, the restoring material should present mechanical properties to support masticatory forces and to resist to the wear[8,13] In general, the materials more used are the adhesive systems, the composite resins, the cements of glass ionomer[12,22-24] or a combination of techniques[25,26].

Before the exposed, the aim of this study was the biomechanical behavior analysis of the abfraction lesion in mandibular central incisor tooth (MCIT), within wedge-shaped lesion simulating abfraction lesion, to evaluate the displacement and stress distribution by means of Laser Speckle (LS) and 3D Finite Element Analysis (FEA), and then compared the results,

advantages and disadvantages of each technique to develop a better understanding of the NCCLs that are fundamental in planning preventive and restorative approach.

2 Material and Methods

A mandibular central incisor tooth (MCIT) was cleaned with Gracey periodontal curette 5-6 (Millennium, Sao Paulo, SP, Brazil) and immersed in distilled water at 37°C until use. The cavity preparation of type V class was made on the buccal, simulating the shape of the abfraction lesions with a cylindrical tip diamonds in 3100 (KG Sorensen, Barueri, SP, Brazil) mounted on high-rotation turbine (Dabi Atlante, São Paulo, SP, Brazil) under constant refrigeration. The cavity was set at 2.0 mm for the occlusal-gingival height, 3.3 mm in mesiodistal length and 2.0 mm axial depth, considering the deepest point of the preparation[27,28] The angle cavosurface was located in all dentin.

The gingival margin of a chopper 28 (SSWhite-Duflex, Rio de Janeiro, RJ, Brazil) was used for the finish. The prophylaxis of cavities was performed with rubber cup (KG Sorensen, Barueri, SP, Brazil) mounted on the handpiece low speed (Kavo Brazil, Joinville, SC, Brazil) and slurry of pumice (SS White-Duflex, Rio de Janeiro, RJ, Brazil). Then, the tooth was embedded in cylindrical tube of polyvinyl chloride (PVC) of 12 mm height, 20 mm diameter, 3 mm thick and filled with chemically activated acrylic resin (JET- Artigos Odontológicos Clássico Ltda, Campo Limpo Paulista, SP, Brazil). The gingival wall of the cavity preparation maintained a distance 1.3 mm from the top edge of the tube and the bottom edge of 2 mm. The tooth was embedded in order to enable the touch of the rod loading application to the tooth.

2.1 LASER SPECKLE

Speckle occurs when coherent light is scattered by a rough surface. In the beginning, it were considered optical noise, but it has been shown a capacity of retain information about the illuminated sample, such as displacements, deformations and biological activity. Other important points are the non-contact, non-destructive and non-invasive treatments to extract information from a sample, and the experimental set-up in most cases is very simple to implement. Usually the light coherent source used is laser, and the speckles could be generated by reflection from a surface, or transmission through a sample. The use of speckle is related to applications in a great range of areas, as metrology[29], rough surfaces study[30], and activity verification of biological tissues[31], food[32] and surfaces[33]. The observed appearance of the speckle is similar to a granulated image, observing points with variable intensity at the register medium, or in a screen.

Speckle interferometry is the application of interference to register a superimposed speckle pattern of an object or medium, resulting in a speckle interference pattern. It is a valuable technique to analyze macroscopic parameters[34], and the possibility of fringe analysis makes it a useful tool in dentistry and engineering applications[35]. However, interferometry techniques have requirement for system's stability[36].

Because of the digital cameras, faster than photographic film to capture images, and an

easier computational quantitative analysis applied in the registered speckle patterns digital images, using a mathematical algorithm, Digital Speckle is widely used for applications, to obtain values with experimental or numerical test to verify its efficiency[37,38] There are works dedicated to the implementation of the speckle digital analysis for industry purposes[39], developing and proposing new experimental set-ups using digital speckle methods. Chen and Chiang[40] proposed an experimental set-up using ESPI, with a very simple optical arrangement, including optical components and hardware equipment for acquisition\processing system, and resistant to vibration and noise. The computational processing was considered, observing the full time of the entire process, since the capture of images, the analytical model applied – attempting to the number of calculations - in the processing stage, until the final results, generating the speckle fringes. The results were compared with other parallel experiment involving Moiré technique analysis, in the same region of the application of the digital speckle, in the sample. However, the analogical film registered pattern has greater resolution (measured in lines/mm), compared to the CCD camera. Other experiments in digital speckle implement and develop analysis methods[41,42], as a consequence of computational hardware capacity.

In this work were implemented the speckle photography technique, using a photographic film, located inside a photographic camera, to record the speckle pattern - each of them obtained for one point and load charge of the sample. This work studies the mechanical behavior of the MCIT using speckle pattern analysis. Similar works were made[43,44], but studying other structures, and comparing experimental values using finite elements method.

The experimental part consists in the recording of the interference pattern and its projection. The speckle interferometer used[45] is composed of a laser source, the sample (MCIT), camera lens and photographic machine (Fig. 1a). The laser strikes the MCIT, generating the speckle, fixed in an apparatus basement developed to apply the load charges using weights, simulating the bite. The camera lens projects the speckle at the photographic camera, which makes the recording process in the photographic film inside it. Taking two speckle patterns, one before and the other after applying different load charges, resulting in the movement of the MCIT, we record the speckle interference pattern at the film. One should attempt to the time exposure, to sensitize correctly it.

After the register stage, we have the reading stage, in which we observe and read information in the speckle interference pattern. The experimental components used are laser, microscopic objective, a first lens to collimate the expanded beam, the speckle film and a second lens to project in a screen the fringes of the speckle interference pattern (Fig. 1b). Measuring the distance between fringes, the corresponding MCIT displacement is obtained, according to the load charge applied and using an appropriate equation.

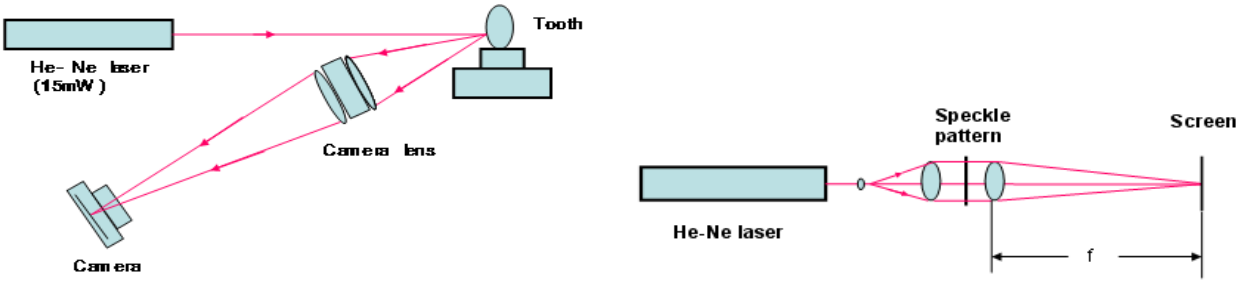

(a) (b)

Fig. 1 Optical systems for (a) speckle recording and (b) Extraction of the displacement interference fringes.

The MCIT attached in the resin was fixed in an Aluminum basement, which has an iron tip connected in a flagpole, responsible for the simulation of the bite (Fig. 2). Were applied charge forces between 10.21N and 40.21N (additional weight of 0.21kg due to iron tip) in a small area (less than 1 mm^2), with angle 15° with respect to the long axis of the MCIT.

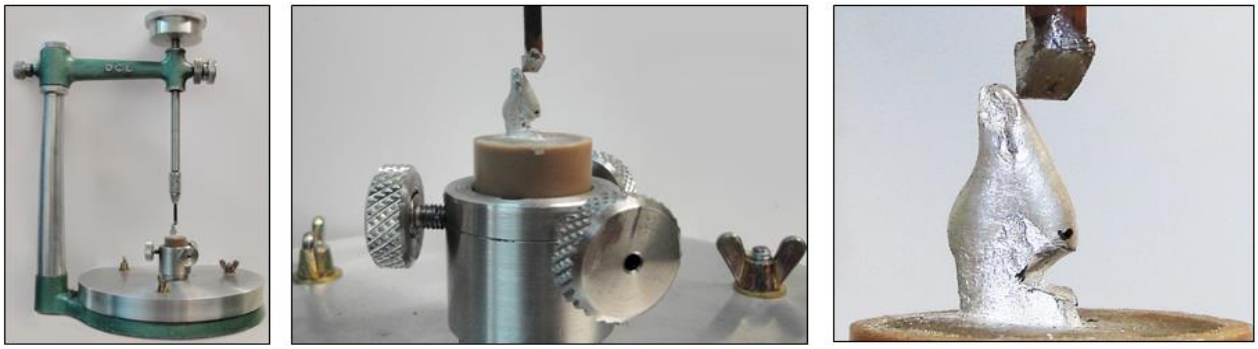

a b c

Fig. 2 (a) Experimental set up to apply loads in the tooth, (b) tooth adjusted and fixed in the base and (c) close view of the tooth and the applied force area.

The study area was illuminated with light of He-Ne laser (15 mW, λ= 632.8 nm, Melles - Griot). A special photographic film (Fuji Minicopy Film HR II) was positioned inside a photographic camera Nikon FM10 to record the patterns, and the objective lens of the same camera were used. The Figs. 3a-3c shows the experimental setup. The speckle is applied in two parts of the MCIT: in the abfraction point (crack region) and the other above the same (upper position of the crack region), using four weights as loading charges to simulate the bite. Eight speckle pattern films were generated.

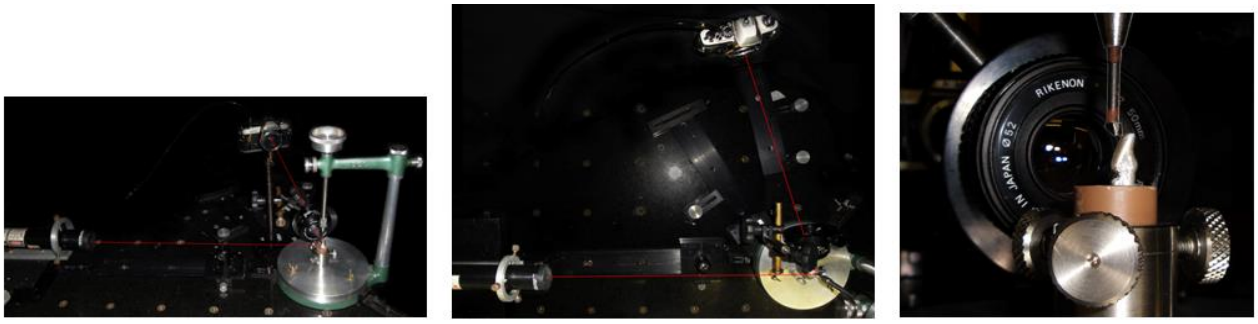

(a) (b) (c)

Fig. 3 Perspective view of the Laser Speckle - general (a), superior (b) and zoom (c).

2.2 FINITE ELEMENT ANALYSIS

The Finite Element Analysis (FEA) is a numerical method based on the construction of a mathematical model, representing geometrically the object to be analyzed. This model is subdivided into a number of cells known as finite elements, in triangular linear or quadratic shape, depending on the geometry of the model and analysis to be performed. Each element is defined by a number of points called nodes. In a three dimensional (3D) model, nodes are localized in a system of orthogonal cartesian coordinates (X, Y, Z) connecting the respective elements. The resulting set is called a mesh, where each one of them are related to the material properties, for example, mechanical properties, like elastic modulus and Poisson's ratio, and the boundaries conditions and loading, helping in the representation of the actual physical model.[46]

The FEA can be divided into three steps: preprocessing, processing stage or solution analysis and pos-processing. In preprocessing, modeling the structure examined (geometric characteristics) and physical characteristics of the materials involved. The structures are discretized by nodes and elements, to then apply boundary conditions and loading. In processing stage, application of an algorithm to solve the system of equations of the problem modeled. In pos-processing, the results generated by processing are displayed.[46]

The processing stage was performed using MSC.NASTRAN2005r1 software (MSC Software Corporation, Santa Ana, CA, USA). The MSC.PATRAN2005r2 software, used in the preprocessing, was also used for pos-processing, visualization, and evaluation of the results. A 3D MCIT model was generated from the tooth's dimensions (dentin and enamel) used in the experimental part. The pulp part was obtained by interpolation, using the mean diameter of the apical foramen[47], and the values for cervical region were based on Shillinburg and Grace[48].

From the surfaces of structures (pulp, dentin and enamel) made up, we obtained the cavity and support structures (Fig. 4a). Next surface meshes were generated with triangular elements of linear flat topology Tri3, one side containing three edges, with one node in each end of the edges. We used elements of edges of size 0.05mm, in regions of high curvature, small size or transition between structures, edged up to 0.75mm in areas of small curvature, of great size or distance between the transition structures, following the procedures in Poiate et al.[3,49-52]. Then, mesh volumetric generation were made, with tetrahedral topology elements Tet4, four-sided pyramidal element containing six edges, with a knot in each end of them (Fig. 4b).

.

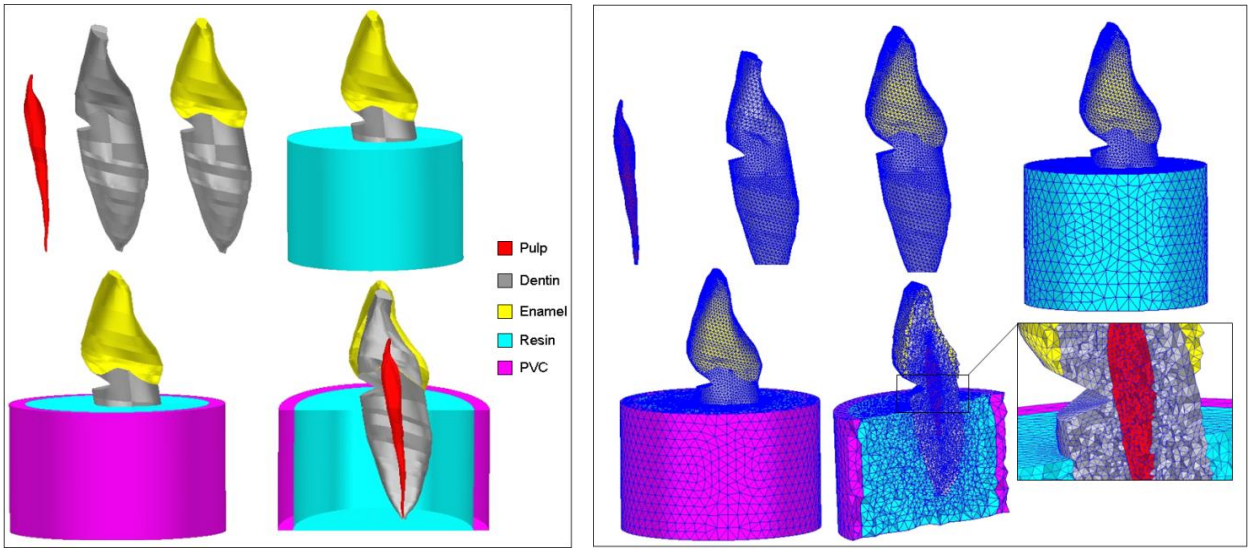

Fig. 4 Generating (a) surfaces of structures and (b) finite element mesh for all structures.

The degree of discretization of the models was established from convergence studies of the results in computer modeling (Pentium Dual-Core processor 2.2 GHz, 160 GB hard drive and 3 GB of RAM memory), to ensure that a proper FE model mesh density was generated. In this way, we were able to ascertain that our system realistically described the anatomic geometry, obtained for the model 334749 elements and 54537 nodal points.

Although the hexahedral elements are better than tetrahedral, considering the solution of the equations and results, they were not used, because of the geometry complexity considered, in which elements would appear distorted, compromising the geometry discretization and analysis.

We assumed that all the structures of the model were homogeneous, isotropic and linearly elastic, characterized by two physical properties: Young's modulus (E) and Poisson's ratio (v) To model the tooth as a single unit, we assumed the interfaces between structures perfectly united. In our aim was to provide an initial justification of our approach, we believed that this simplification was justified[3,49-52] Table 1 lists the values that were used in each of the structures.

Table 1 Mechanical prosperties and references in each anatomical structure.

Structure / Material	Young's Modulus (GPa)	Poisson's Ratio	Reference
Pulp	0.02	0.45	Farah and Craig[52]
Dentin	18.60	0.31	Ko et al[54]
Enamel	41.00	0.30	Ko et al[54]
Acrylic Resin	2.26	0.35	Çifçi & Canay[55]
PVC	2.51	0.36	O'Brien[56]

The boundary conditions, or the setting of the model, and the characteristics of the load application were prepared similarly to the experimental part. The total static load of 42.1 N was distributed by six nodal points in an area of 0.07 mm^2 (Fig. 5).

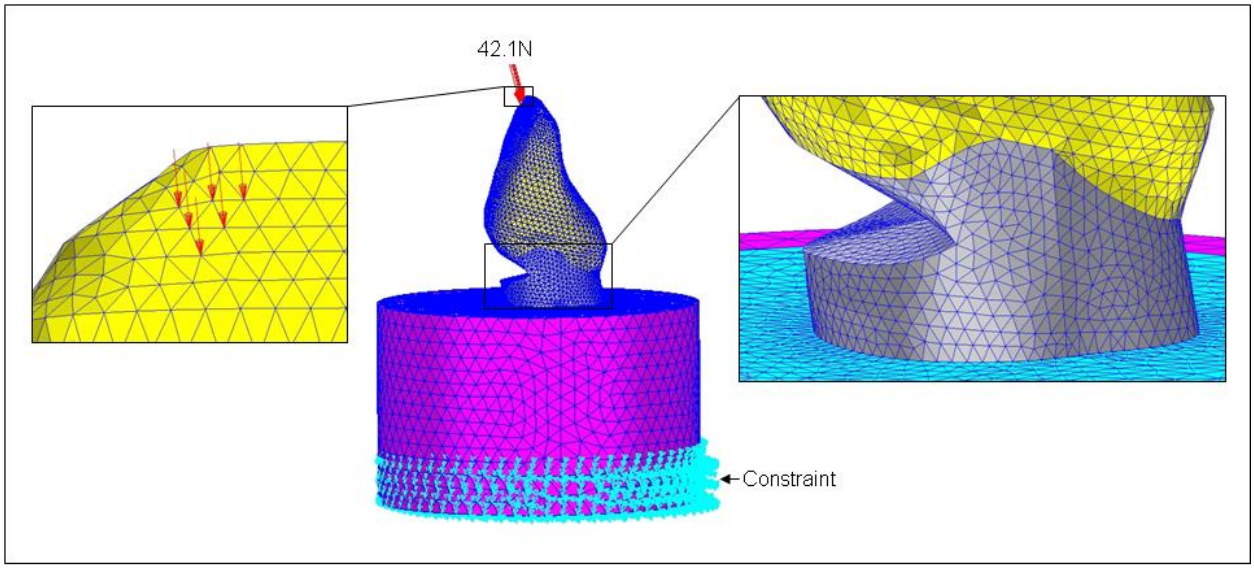

Fig. 5 Boundary conditions in the FE model.

3. Results

3.1 LASER SPECKLE

Fig. 6 show the tooth illuminated by the laser He-Ne, seen through the camera lens, and the respective measurement points in the crack (1) and upper position of the crack (2), related to the experimental setup shown in Fig. 1a and Fig. 3. After the speckle patterns were registered in each photographic film, were performed the observation experiment, related to the observation of the fringes projected in a screen.

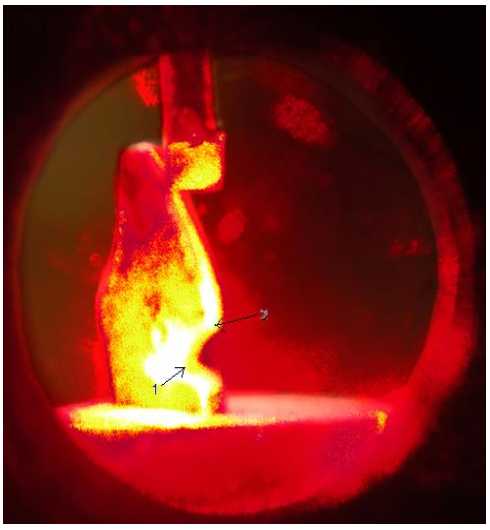

Fig. 6 Tooth illuminated and the points of measurement, in the crack (1) and upper position of the crack (2).

The quantitative analysis of the speckle fringe pattern allow to obtain the MCIT displacement using equation (1), where the relationship between the displacement ΔX_c and the separation *d* of fringes is expressed by[57]:

$$\Delta X_C = \frac{\lambda . f}{m.d} \quad , \qquad (1)$$

where λ is wavelength of the laser, *f* focal length of camera lens, *m* magnification of image in the optical system, and *d* separation between two interference fringes, measured directly in a screen. The results were presented in the table 2, using the constant values of *m*=6.5, λ=0.633μm and *f* =45.1cm in the equation (1).

Table 2 Load, place and results from LS.

Load (N)	Displacement in the crack (μm)	Displacement in upper position of the crack (μm)
12.1	-	-
22.1	-	7.96
32.1	11.5	12.5
42.1	14.4	25.8

The resulting interference fringes of displacement in the crack and at the upper position of the crack are shown in the Figs 7 and 8, respectively.

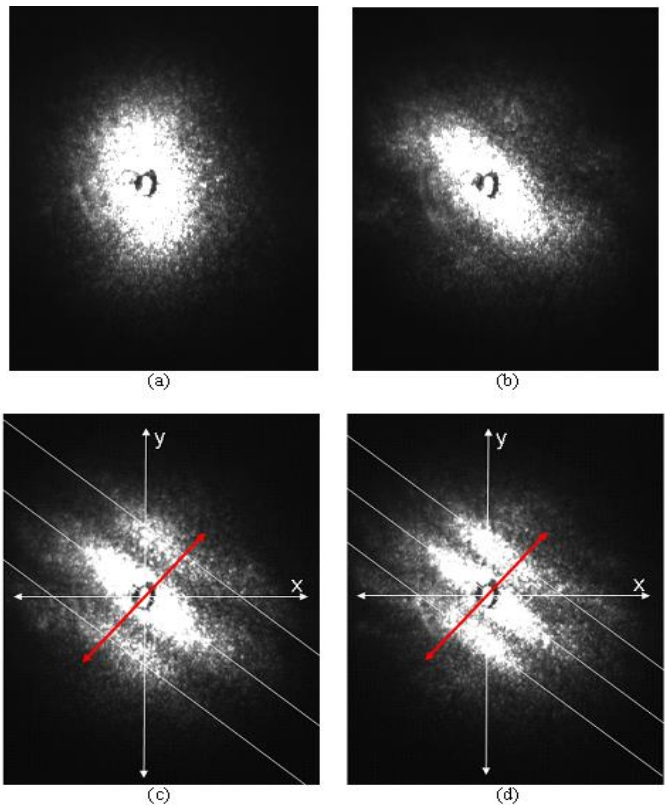

Fig.7 Interference fringes of displacement in the crack: (a) 12.1N, (b) 22.1N, (b) 32.1N and (d) 42.1N.

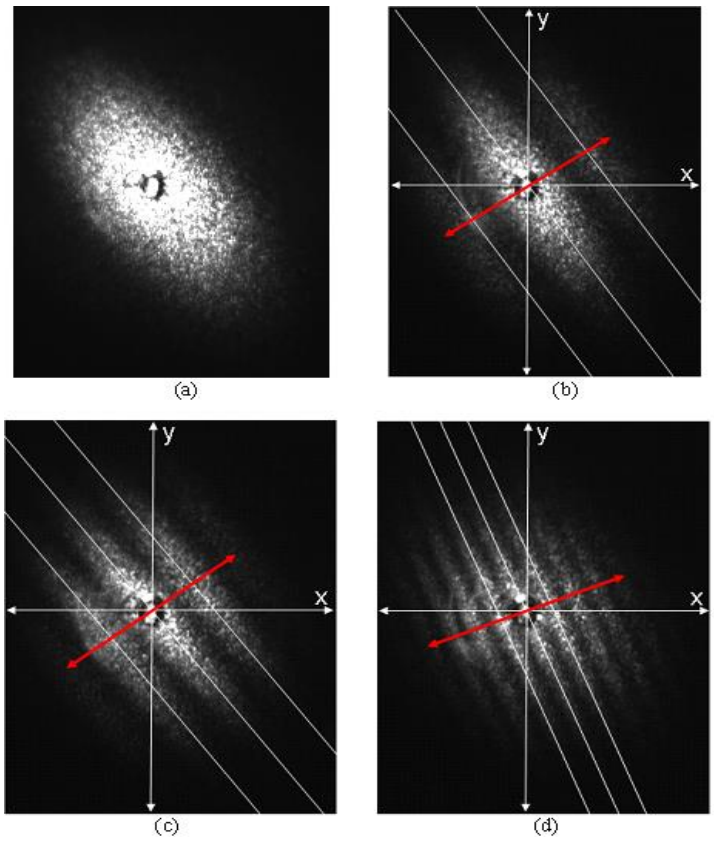

Fig. 8 Interference fringes of displacement at the upper position of the crack: (a) 12.1N, (b) 22.1N, (b) 32.1N and (d) 42.1N.

In Figure 7 the MCIT movement is in one direction (red line) and the fringes being parallel one to the other. Until 22.1N load in the MCIT there is only one fringe in the crack region (Fig. 7a and b) and the displacement cannot be evaluate because is necessary at least two of them to do it. However, when the load is charge to 32.1N, the displacement evaluated is 11.5μm, and when the load increases to 42.1N (31.2%), the displacement result is 14.4μm, that's represent the increase of displacement around 25.2%. The orientation of the superficial displacement, that is perpendicular to the fringes, is the same with 32.1 and 42.1N (Fig. 7 c and d), around 50° in relation the axis x in counterclockwise.

In the upper position of the crack region of the MCIT when the load is 22.1N (Fig. 8b) the displacement evaluated is 7.96μm, and when the load increases to 32.1N (45.2%), the displacement result is 12.5μm, that's represent the increase of displacement around 57%. The orientation of the superficial displacement is 34 and 37°, in relation the axis x in counterclockwise, with 22.1 and 32.1N, respectively (Fig. 8b and c). However, when the load increases (31.2%) from 32.1 to 42.1N, the displacement result is 25.8μm (increase of 106.4%), and the orientation of the superficial displacement in the MCIT change from 37° (Fig. 8c) to 22° (Fig. 8d).

3.2 FINITE ELEMENT ANALYSIS

A panoramic view of the results regarding the Maximum Principal Stress (MPS) distribution are illustrated in Fig. 9, from the complete

view of the model and only the dentin and enamel. The color scale represent stresses in MPa, where positive values are tensile and negative compression stresses. It appears that the region of abfraction the concentration of tensile stresses, the maximum 4 MPa, the same angle of view obtained by LS. The tensile stress at the cavity simulating shape of the lesion abfraction varied from 0.25MPa to 16MPa. The compression stress at the load application area reaches -37MPa, and is distributed in a great extension of the lingual surface, and dissipated in mesial and distal directions.

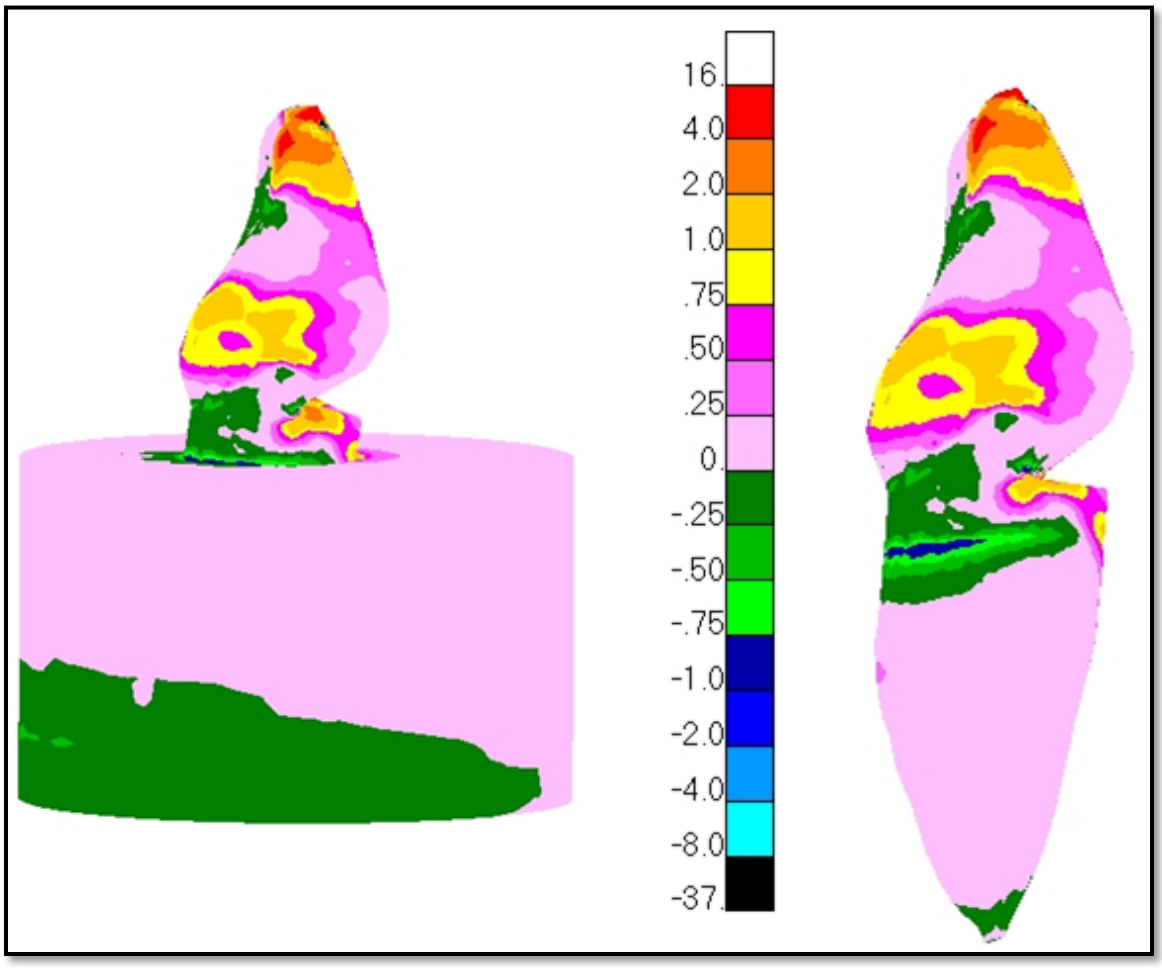

Fig. 9 MPS in the finite element model.

Fig. 10a shows MPS distribution in an opposite angle of view obtained by LS, the maximum value 6 MPa in the region of abfraction. Thus, the maximum stress was concentrated in the cavity simulating the shape of the lesions abfraction near the distal face (contrary to the angle the obtained by LS), because the load that is applied near the mesial face, which was expected because the torsion effect the tooth is subjected.

Fig. 10b shows the displacement obtained by FEA in the MCIT. The color scale corresponds to the displacement in mm. In the region of the occlusal angle cavosurface (upper crack) there was a displacement of 4.5µm.

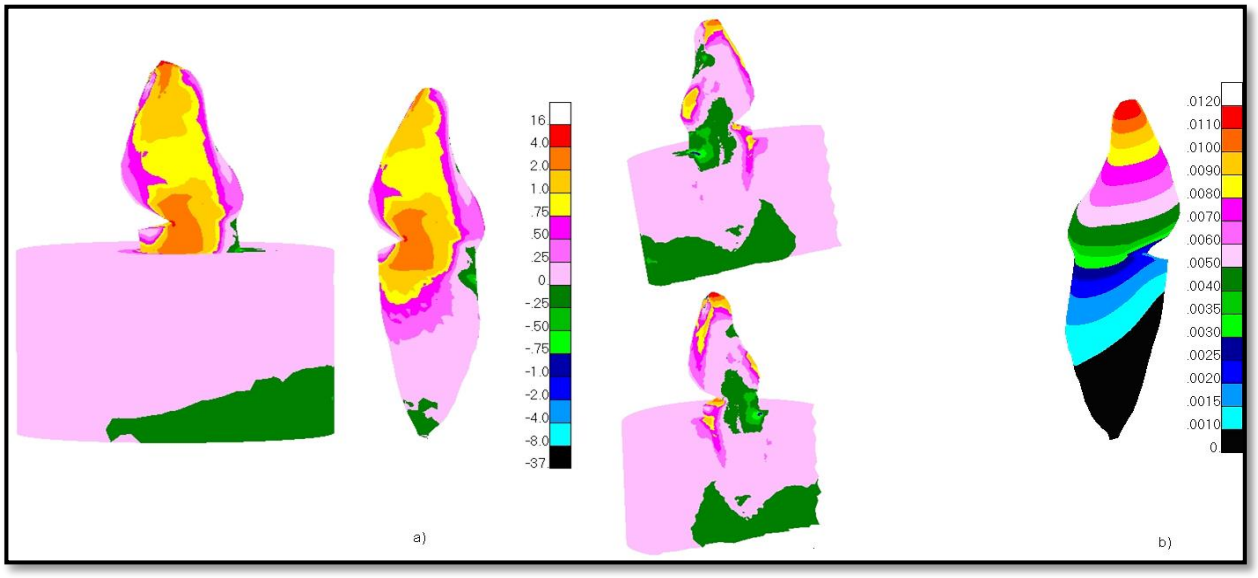

(a) (b)

Fig. 10 (a) MPS in Finite Element model – opposite angle obtained by LS – and (b) Displacement Values.

Fig. 11 shows the displacement vector in MCIT from FEA. The displacement orientation is up to down due to the load and boundary conditions and the regions measured by LS are circled in the FEA. The displacement direction is 37° in relation the axis x in counterclockwise in the occlusal angle cavosurface (upper crack), and in the inner region of the wedge (crack) is 50°. These results represent an excellent agreement with LS until 32.1N.

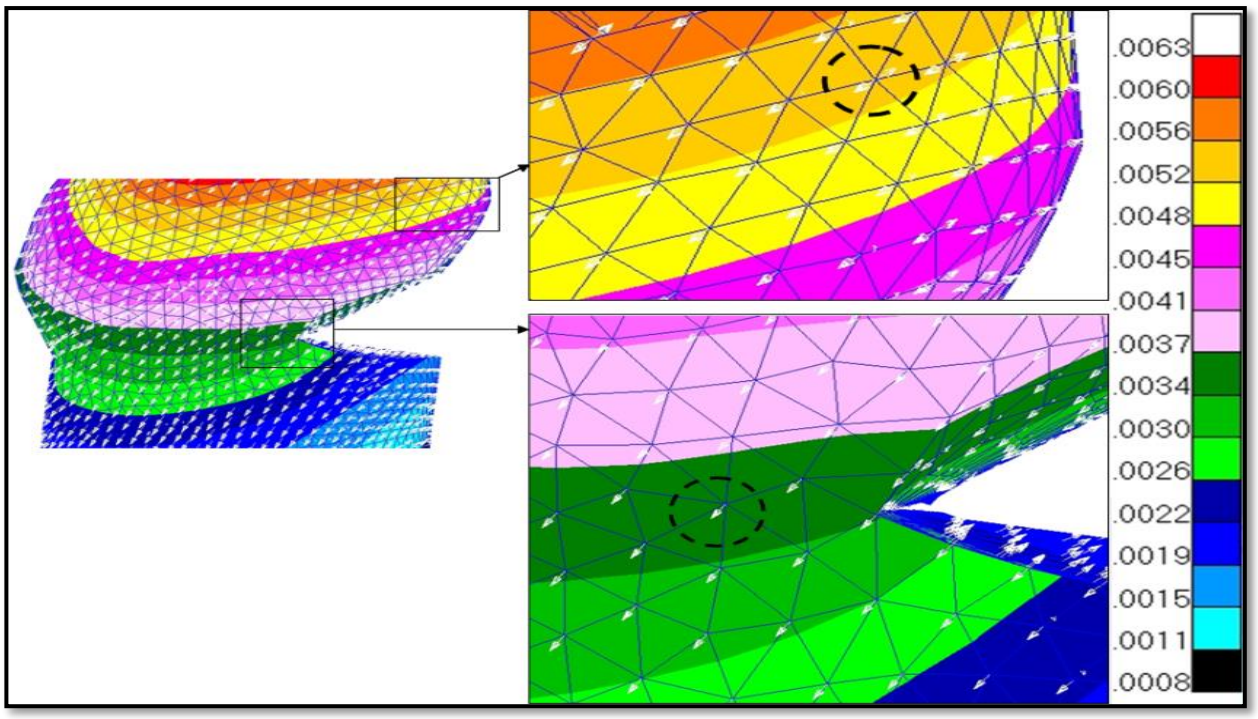

Fig. 11 Displacement vector in the FEA.

4. Discussion

Many of the cervical defects thought to be extrinsic factors acting directly upon the tooth surface are actually due to eccentrically applied occlusal forces, such as sharp, angular or wedge-shaped defects[4,5,15,58]

In spite of in the critical review by Barlett and Shaw[2], it is postulated that there is still little evidence correlating abfraction and occlusion stress (just from FE analysis and lab work), with some previous clinical investigations have proven it[11,12,15,59,60] Tensile stress may cause disruption of the bonds between hydroxyapatite crystals, leading to cracks in the enamel and eventual loss of enamel and the underlying dentine.[4,20,58,61,62]

The representation of a MCIT is based on evidences from studies[9,63], which demonstrate such lesions are most commonly found in upper incisors, followed by premolars and, least commonly, teeth canines.

4.1 LASER SPECKLE

The nonlinear behavior in the displacements and the change of axial orientation, apart from 32.1N, could be due to MCIT nonlinear behavior and instabilities in the region of measurement process, which is prone to produce a large displacement, compared the crack region, due to the abfraction geometry (lesion) and distance of the loading application from the fixed region, near the base of the tooth.

We have more values of displacement obtained from the upper position of the crack than the region of the crack in the MCIT, and, for the same force applied, the values are greater in one case than the other. For 32.1N loading in the MCIT, there is a difference of 8.7% between the two values; however, when the load is 42.1N, the resulting difference is of 79.2%.

We observe the stable behavior of the displacement's movements, the direction is the same in the region of the crack, while in the upper position of the crack it did not happen. There is more stability in one region than the other, one of them distant from the basement, and the torque effect is stronger in it: the nearest of the basement of the MCIT, the more stable the movement will be.

4.2 FINITE ELEMENT ANALYSIS

The stress profiles seem to mimic the pattern of clinical presentation of abfraction lesions[4, 5,13] Patterns of stress distribution near the cavity, simulating the shape of the lesions abfraction, may also be explained by the location, lever effect and orientation of load application, which cause forces that generate tensile stresses at the cavity, simulating shape of the lesions abfraction, because they tend to deflect the tooth in the lingual direction.

An interesting finding was the stress concentration at the cavity, simulating shape of the lesions abfraction, being lower in the enamel than in cervical dentine. A factor that must be considered is the difference between the Young's Modulus, since the rigidity of enamel is higher than the dentine, the enamel concentrates the stresses that are dissipated by the dentine. It is well known that enamel and dentine respond differently to masticatory stresses. Although these tissues are intended to support each other, they can react to occlusal forces independently. Dentine has shown low compressive and high tensile stresses, while enamel has demonstrated a reverse trend.

4.3 LASER SPECKLE VERSUS FINITE ELEMENT ANALYSIS

The displacement obtained by FEA in the MCIT in the region of the occlusal angle cavosurface (upper crack) there was a displacement of 4.5μm, 5.7 times smaller than the measured by LS (25.8μm), under the same load. In the inner region of the wedge (crack) the displacement is 3.5μm, 4.1 times smaller than the measured by LS. This difference between LS and FEA could be due to the difference between the mechanical properties of the real and the simulated model and the nonlinear behavior in the MCIT, apart from 32.1N, observed in the LS.

It is worth mentioning that up to 31.2N load the displacement direction results in the occlusal angle cavosurface, and in the inner region of the wedge from LS and FEA results represent an excellent agreement.

This study has found that the buccal stress concentration in a MCIT were higher at the gingival region due to occlusal overload. Considering the tooth flexure theory, this finding suggests biomechanical explanations to MCIT are one of the teeth more prone to develop clinically abfraction lesions. However, the other factors implicated in cervical lesions like attrition, erosion, abrasion, must be evaluated and studied further to support the previous researches using FEA and other techniques[64].

Therefore, to develop a better understanding of the cervical lesion, relevant to the clinical treatment, analyses of the stress distribution in the teeth are highly desirable to evaluate the degree of these NCCLs and recognize that progressive changes in the cervical area of the tooth are part of a physiologically dynamic process that occurs with aging. Thus, the clinical decision to treatment plan with preventive and restorative approach of the NCCLs, with the technique and materials to be used appropriately, may be based on the need to replace form and function or to relieve hypersensitivity of severely compromised teeth or for esthetic reasons, for control of the disease, preventing the appearance of new lesions and guaranteeing a better quality of life to the patient[65-69].

5. Conclusion

Among the advantages and disadvantages of each technique, Laser Speckle (LS) has an easy and simple experimental setup, which can be performed quickly and get the results in the real model, but is not possible to achieve results in certain areas of difficult access, and if we want to obtain results at several points simultaneously, multiple CCD's are necessary. Using Finite Element Analysis FEA, we are able to visualize the stress, strain and displacement at any location, but it is very difficult to construct and simulate the boundary conditions of the real physical model, which depends on the mechanical properties, material behavior and the conditions adopted in the numerical simulation. Both techniques showed good agreement in many aspects, for example, in the displacement direction, and were complementary to the understanding of the results, and it is recommended they be used concurrent, especially as most of the FEA disadvantages have been overcome. Given the limitations of the study, there was a good agreement qualitatively between the two methods applied, the LS and FEA. However, many studies continue must be developed in

the improvement of methodology and techniques, like the use of Electronic Speckle Pattern Interferometry (ESPI) and strain gauge (SG), because knowledge of the distribution of stress, strain and displacement are fundamental importance in planning interventions in abfraction lesions.

Acknowledgement:

The authors are grateful to the CAPES (Coordenação de Aperfeicoamento de Pessoal de Nível Superior, Coordination for the Improvement of Higher Education Personnel) by the funding source.

Funding Statement:

None

Conflicts of Interest Statement:

None

References:

1. Pereira AFV, Poiate IAVP, Poiate Jr E, Miranda Jr WR. Abfraction lesions revisited: Contemporary Concepts and Therapeutic Measures. *Rev. Gaúcha Odont.* 2008;36:321-326.

2. Barttlet DW, Shah P. A critical review of non-carious cervical (wear) lesions and the role of abfraction, erosion, and abrasion. *J. Dent. Res.* 2006;85:306-312.

3. Poiate IAVP, Vasconcellos AB, Poiate Jr E, Dias KRHC. Stress distribution in the cervical region of on upper central incisor in a 3D finite element model. *Braz. Oral. Res.* 2009;23:161-168.

4. Lee WC, Eakle WS. Possible role of tensile stress in the etiology of cervical erosive lesions of teeth. *J. Prosth. Dent.* 1984;52:374–380.

5. Grippo JO. Abfractions: a new classification of hard tissue lesions of teeth. *J. Esthet. Dent.* 1991;3:14-19.

6. Kuroe T, Itoh H, Caputo AA, Konuma M. Biomechanics of cervical tooth structure lesions and their restoration. *Quint. Int.* 2000;31:267-274.

7. Kuroe T, Itoh H, Caputo AA, Nakahara H. Potential for load-induced cervical stress concentration as a function of periodontal support. *J. Prosth. Dent.* 1999;11:215–222.

8. Lee WC, Eakle WS. Stress-induced cervical lesions: review of advances in the past ten years. *J. Prosth. Dent.* 1996;75:487-494.

9. Rees JS. The role of cuspal flexure in the development of abfraction lesions: a finite element study. *Eur. J. Oral Sci.* 1998;106:1028-1032.

10. McCoy G. The etiology of gingival erosion. *J. Oral Implantol.* 1982;10:361-366.

11. Peaumans M, De Munck J, Landuyt V, Kanumilli P, Yoshida Y, Inoue S, et al. Restoring cervical lesions with flexible composites. *Dent. Mater.*2007;23:749-754.

12. Burke FJT, Whitehead SA, McCauguey AD. Contemporary concepts in the pathogenesis of the Class V non-carious lesion. *Dent. Update.* 1995;22:28-32.

13. Heymann HO, Sturdevant JR, Bayne SC, Wilder AD, Sluder TB, Brunson WD. Examining tooth flexural effects on cervical restorations: a two-year clinical study. *J. Am. Dent. Assoc.* 1991;122:41–47.

14. Goel VK, Khera SC, Singh K. Clinical implications of the response of enamel and dentin to masticatory loads. *J. Prosthet. Dent.* 1990;64:446-454.

15. Leinfelder KF. Restoration of abfracted lesions. *Compendium.* 1994;15:1396-1400.

16. Alani AH, Toh CG. Detection of microleakage around dental restorations: a review. *Oper. Dent.* 1997:22:173-185.

17. Braem M, Lambretchs P, Vanherle G. Stress-induced cervical lesions. *J. Prosthet. Dent.* 1992;67:718-722.

18. Lambrechts P, Braem M, Vanherle G. Evaluation of clinical performance for posterior composite resin adhesives. *Oper. Dent.* 1987;12:53-78.

19. Manhart J, Chen HY, Mehl A, Weber K, Hickel R. Marginal quality and microleakage of adhesives class V restorations. *J. Dent.* 2001;29:123-130.

20. Grippo JO. Noncarious cervical lesions: the decision to ignore or restore. *J. Esthet. Dent.* 1992;4:55-64.

21. Kirveskari P, Jämsä T, Alanen P. Occlusal adjustment and the incidence of demand for temporomandibular disorder treatment. *J. Prosthet. Dent.* 1998;79(4):433-438.

22. Baratieri LN, Canabarro S, Lopes GC, Ritter AV. Effect of resin viscosity and enamel beveling on the clinical performance of class V composite restorations: three-years results. *Oper. Dent.* 2003;28:482-487.

23. Browning WD, Brackett WW, Gilpatrick RO. Two-year clinical comparison of a microfilled and a hybrid resin-based composite in non-carious class V lesions. *Oper. Dent.* 2000;25:46-50.

24. Van Meerbeek BV, De Munck J, Yoshida Y, Inoue S, Vargas M, Vijay P, et al. Adhesion to enamel and dentin: current status and future challenges. *Oper. Dent.* 2003;28:215-235.

25. Gladys S, Van Meerbeek BV, Lambrechts P, Vanherle G. Marginal adaptation and retention of a glass-ionomer, resin-modified glass-ionomers and a polyacid-modified resin composite in cervical class-V lesions. *Dent. Mater.*1998;14:294-306.

26. Gladys S, Van Meerbeek B, Lambrechts P, Vanherle G. Evaluation of esthetic parameters of resin-modified glass-ionomer materials and a polyacid-modified resin composite in class V cervical lesions. *Quint. Int.* 1999;30:607-614.

27. Fruits TJ, VanBrunt CL, Khajotia SS, Duncanson Jr MG. Effect of cycling lateral forces on microleakage in cervical resin composite restorations. *Quint. Int.* 2002;33:205-212.

28. Schneider LFJ, Tango RN, Milan FM, Mundstock GV, Consani S, Sinhoreti MAC. Microleakage evaluation of composite restorations submitted to load cycling. *Cienc. Odontol. Bras.* 2004;7:27-33.

29. Muramatsu M, Lunazzi JL. Advantages of a derivative technique in performing speckle correlations. *Appl. Opt.* 1984;23(18):3038-3039.

30. Rebollo MA, Landau MR, Hogert EN, Gaggioli NG, Muramatsu M. Roughness determination by direct visual observation of the speckle pattern. *Opt. Laser Tech.* 1995;27(6):355-356.

31. Silva Jr E, Silva ERT, Muramatsu M, Lannes SCS. Transient process in ice creams evaluated by laser speckles. *Food Res. Int.* 2010;43:1470-1475.

32. Nieri TM, Peres MAO, Silva ER, Fabbro IMD, Muramatsu M, Andreollo NA. The optical analysis of the abdominal wall using the biospeckle after implants of polypropylene mesh in rats. *Acta Cir. Bras.* 2009;24(6):442-448.

33. Muramatsu M, Guedes GH, Gaggioli NG. Speckle correlation used to study the oxidation process in real time. *Opt. Laser Tech.* 1994;26(3):167-168.

34. ERF R (ed.). Speckle Metrology. Academic Press;1978.

35. Ruiz PD, Kaufmann GH, MoK O, Galizzi GE. Evaluation of impact-induced transient deformations using double-pulsed electronic speckle pattern interferometry and finite elements. *Opt. Lasers Eng.* 2000;32:473-484.

36. Nicoletto G, Anzelotti G, Riva E. Mesoscopic strain fields in woven composites: Experiments vs. finite element modeling. *Opt. Lasers Eng.* 2009;47:352-359.

37. Tyrer JR, Petzing JN. In-plane Electronic Speckle Pattern Shearing Interferometry. *Opt. Lasers Eng.* 1997;26:395-406.

38. Ruiz PD, Kaufmann GH, Möller O, Galizzi GE. Evaluation of impact-induced transient deformations using double-pulsed electronic speckle pattern interferometry and finite elements. *Opt. Lasers Eng.* 2000;32:473-484.

39. Aebischer HA, Waldner S. Strain distributions made visible with image-shearing speckle pattern interferometry. *Opt. Lasers Eng.* 1997:26:407-420.

40. Chen DJ, Chiang FP. Computer-aided speckle interferometry using spectral amplitude fringes. *Appl. Opt.* 1993;32(2):225-236.

41. Huntley JM. Fast transforms for speckle photography fringe analysis. *Opt. Lasers Eng.* 1986;7(3):149-161.

42. L. B. Meng, G. C. Jin, X. F. Yao, Application of iteration and finite element smoothing technique for displacement and strain measurement of digital speckle correlation. Opt. Lasers Eng. **45,** 57-63 (2007).

43. J. W. Tong & Y. Na, A Study of Stress Propagation Under Impact Loading Using Double Exposure Speckle Photography and Finite Element Analysis. Opt. Lasers Eng. **12** 35-42 (1990).

44. R. González-Peña, R.M.C.O Anda, A. J. Pino-Velázquez, Y. González-Jorge, R. Salvador-Palmer, Determination of strain and stress distribution on shearwalls by using the speckle photography technique. Opt. Lasers Eng. **39,** 609-618 (2003).

45. J.C. Dainty (ed.): Laser Speckle and Related Phenomena (Springer-Verlag 1975).

46. K.J. Bathe: An introduction to the use of the finite element procedures in Finite Element Procedures, 3th ed. (Prentice-Hall, Englewood Cliffs, New Jersey 1996).

47. D. Green, N.Y. Brooklyn, Stereomicroscopic study of 700 root apices of maxillary and mandibular posterior teeth. Oral. Surg. Oral Med. Oral Pathol. **13,** 728-33 (1960).

48. H.T. Shillingburg, C.S. Grace, Thickness of enamel and dentin. J. South Calif. Dent. Assoc. **41,** 33-52 (1973).

49. I.A.V.P. Poiate, A.B. Vasconcellos, A. Andueza, I.R.V. Pola, E. J. Poiate, Three dimensional finite element analyses of oral structures by computerized tomograghy. J. Biosc. Bioeng. **106,** 906-909 (2008).

50. I.A.V.P. Poiate, A.B. Vasconcellos, R.B. Santana, E. Poiate Jr, Three-dimensional stress distribution in the human periodontal ligament in masticatory, parafunctional, and trauma loads: finite element analysis. J. Periodont. **80**, 1859-1867 (2009).

51. I.A.V.P. Poiate, A.B. Vasconcellos, E. Poiate Jr, K.R.C Dias, Stress distribution in the cervical region in a 3D FE. Braz. Oral Res. **23,** 161-168 (2009).

52. I.A.V.P. Poiate, A.B. Vasconcellos, M. Mori, E. Poiate Jr, 2D and 3D finite element analysis of central incisor generated by computerized tomography. Comput. Meth. Prog. Biomed. **104(**2), 292-9 (2011).

53. J.W. Farah, R.G. Craig, Reflection of photoelastic stress analysis of a dental bridge. J. Dent. Res. **53**, 859-866 (1974).

54. C.C. Ko, C.S. Chu, K.H. Chung, M.C. Lee, Effects of post on dentin stress distribution in pulpless teeth. J. Prosthet. Dent. **68** 421-427, (1992).

55. Y. Çiftçi, S. Canay, The effect of veneering materials on stress distribution in implant-supported fixed prosthetic restorations. Int. J. Oral Maxillofac. Implants **15,** 571-582 (2000).

56. W.J. O'Brien, University of Michigan. NIDR Materials Science Research Center at the University of Michigan School of Dentistry. Biomaterials Properties Database [homepage on the Internet] [accessed 2015 Jan 1; Revised April, 1997]. Available from: http://www.zubnistranky.cz/intro.html.

57. E. Archbold & A.E. Ennos, Displacement measurement from double-exposure laser photographs. Optica Acta **19**, 253-271 (1972).

58. V.F. Ferrario, C. Sforza, G. Serrao, C. Dellavia, G.M. Tartaglia, Single tooth bite forces in healthy young adults. J. Oral Rehabil. **31** 18–22, (2004).

59. O. Bernhardt, D. Gesch, C. Schwahn, F. Mack, G. Meyer, U. John, et al, Epidemiological evaluation of the multifactorial aetiology of abfractions. J. Oral Rehabil. **33** 17- 25, (2006).

60. H.A. Lyttle, N. Sidhu, B. Smyth, A study of the classification and treatment of noncarious cervical lesions by general practioners. J. Prosthet. Dent. **79,** 342-6 (1998).

61. J.S. Rees, M. Hammadeh, D.C. Jagger, Abfraction lesion formation in maxillary incisors, canines and premolars: a finite element study. Eur. J. Oral Sci. **111**, 149–154 (2003).

62. E.B. Las Casas, T.P. Cornacchia, P.H. Gouvêa, C.A. Cimini, Abfraction and anisotropy – effects of prisms orientation on stress distribution. Comput. Methods Biomech. Biomed. Engin. **6,** 65-73 (2003).

63. J.S. Rees, M. Hammadeh, Undermining of enamel as a mechanism of abfraction lesion formation: a finite element study. Eur. J. Oral Sci. **112**, 347-352 (2004).

64. Stănuș A et al. Morphological and Optical Coherence Tomography Aspects of Non-Carious Cervical Lesions. *J. Pers. Med.* 2023, 13, 772.

65. Nascimento MN et al. Abfraction lesions: etiology, diagnosis, and treatment options. Clinical. *Cosmetic and Investigational Dentistry*. 2016;8:79-87.

66. El-Marakby et al. Noncarious Cervical Lesions as Abfraction: Etiology, Diagnosis, and Treatment Modalities of Lesions: A Review Article. *Dentistry* 2017, 7:438.

67. Mathias C et al. Treatment of non-carious lesions: Diagnosis, restorative materials and techniques. *Braz Jour Oral Sc.* 2018;17: e18336.

68. Roberts WE, Mangum JE, Schneider, PM. Pathophysiology of Demineralization, Part I: Attrition, Erosion, Abfraction, and Noncarious Cervical Lesions. *Curr Osteoporos Rep.* 2022;20:90–105.

69. Goodacre CJ, Eugene Roberts W, Munoz CA. Noncarious cervical lesions: Morphology and progression, prevalence, etiology, pathophysiology, and clinical guidelines for restoration. *J Prosthodont.* 2023;32:e1–e18.